applied sciences

MDPI

Article

Integrated Adaptive Steering Stability Control for Ground Vehicle with Actuator Saturations

Jinhua Zhang [1,†] and Mingyu Wang [2,*,†]

[1] School of Mechanical and Electrical Engineering, Guangzhou University, Guangzhou 510006, China
[2] School of New Energy, Nanjing University of Science and Technology, Jiangyin 214331, China
* Correspondence: mingyu@njust.edu.cn
† These authors contributed equally to this work.

Abstract: During a steering manoeuvre in a ground vehicle, both yaw motion and roll motion can occur simultaneously, and their dynamics can be coupled, as the roll motion is generalized directly from the tires' lateral force under steering. Hence, it is of significance to analyze them as an integrated plant in the vehicle steering stability control problem. Furthermore, the actuator saturation of yaw control cannot be neglected, as vehicles often steer at a high velocity or on low-friction roads. In this paper, an integrated steering dynamics model is established considering the coupling between the roll motion and lateral motion, then a novel nonlinear adaptive controller is proposed to stabilize the steering motion considering the actuator saturation of yaw motion control. Simulation results indicate that the designed integrated controller is effective in improving the performance of both the yaw rate tracking error and ride comfort taking into account vehicle parameter uncertainties and actuator saturation; the steering stability of ground vehicles can consequently be guaranteed.

Keywords: vehicle integrated control; steering stability control; adaptive control; actuator saturations

Citation: Zhang, J.; Wang, M. Integrated Adaptive Steering Stability Control for Ground Vehicle with Actuator Saturations. *Appl. Sci.* **2022**, *12*, 8502. https://doi.org/10.3390/app12178502

Academic Editors: Bo Zhao, Xuejing Lan and Zhiwei Hou

Received: 14 July 2022
Accepted: 24 August 2022
Published: 25 August 2022

1. Introduction

In a steering manoeuvre for a ground vehicle, yaw motion can be generated directly [1,2]. When the vehicle is moving a a high velocity during a steering manoeuvre, unstable sideslip or even drift may occur, which is a dangerous working condition as the vehicle cannot be controlled easily by the driver [3,4]. Consequently, steering stability control is imperative. Conventionally, two signals are taken as controlled states; one is yaw rate, which represents manoeuvrability, while the other is the sideslip angle, denoting lateral stability [5] A novel triple-step nonlinear method was designed for steering stability control of in-wheel motor electric vehicles in [6], realizing the decoupling of the yaw rate and sideslip angle nonlinear dynamics. There have been many steering stability control methods proposed, including the aforementioned paper and others [7–9]; while the control results to date have been brilliant, no influence on vehicle roll motion from steering motion is considered in the extant literature. As is well known from experience, vehicle steering can result in body roll motion, which is related to passenger ride comfort.

As os known, an effective approach to improving passenger ride comfort is an active suspension system (ASS), the principle of which is to isolate the vibration of the unsprung mass to the vehicle body [10,11]. The classical ASS controller is designed based on a quarter-vehicle model [12]. In [13], a multi-objective control was derived for an uncertain nonlinear ASS, taking into account both the dynamic tire load and suspension space. However, the roll motion cannot be handled by a quarter-vehicle model despite the favorable isolation effect of the unsprung mass vibration. Often, vehicle roll stability control is involved in vehicle attitude control, for which a full-car model is most often employed. An adaptive robust ASS controller was develop in [14] using a full-car model, with the roll stability is taken as one of the control targets. The aforementioned roll stability control presents excellent roll stability performance; nevertheless, the roll dynamics effect from vehicle

steering is not involved. Therefore, a nominal roll stability controller that does not consider the effect from steering may not work as desired.

Several researchers have focused on integrated steering stability control. In [15,16], the authors employed a linear quadratic regulator and a sliding mode control method to simultaneously control roll and yaw motion, respectively. A nonlinear control law was designed in [17] to follow the desired trajectories of both yaw and roll behaviours. In [18,19], the authors used model predictive control to simultaneously regulate yaw motion and stabilize roll motion. Similarly, feedback linearization methods have been utilized to solve the coupled yaw–roll motion problem in [20,21]. Although these techniques can handle integrated steering control remarkably well, actuator saturation has not yet been considered. Generally, the yaw stability control moment is realized by active steering or differential braking. When a ground vehicle steers on a low friction road or with a large yaw rate, the tire–road utilized adhesion force cannot supply enough control energy for its physical limitations, which means that saturation of the actuator effort (the active steering angle or braking force) occurs. Hence, it is important to consider the actuator saturation of yaw control in the development of controller design. Two approaches are available to handle actuator saturation: the first is the one-step approach, in which actuator saturation is taken as a constraint in the controller design process [22,23]; the other is two-step approach, in which the nominal controller is designed first, than an anti-windup compensator is designed to handle the actuator saturation [24,25]. Here, we mentions a few approaches: an anti-windup compensator in the form of a filter was designed for an attitude controller in spacecraft under input saturation and measurement uncertainty in [26,27], an auxiliary anti-windup compensator system was introduced to analyze the effect of the input constraint in a saturated robust adaptive backstepping controller design; finally, in this paper, a two-step approach controller is designed to handle actuator saturation.

Based on the aforementioned analysis, a steering stability control system integrating yaw, roll, and lateral and heave movement behaviours with actuator saturation and vehicle parameter perturbations has not previously been studied simultaneously and thoroughly. Thus, an integrated steering stability controller is developed in this paper, taking into consideration parameter perturbations and saturation of the yaw control effort. The main contributions of this paper are summarized as follows: (i) based on the integrated dynamics model, an integrated adaptive steering stability controller is proposed to stabilize the yaw, roll, heave, and lateral motion simultaneously with parameter perturbations; (ii) the actuator saturation of the yaw moment is considered in the context of integrated controller development; hence, the designed controller can guarantee tracing performance of the yaw rate with less degradation.

The rest of this paper is organized as follows: we establish the integrated dynamics model and the analysis of the coupling principle in Section 2; then, we describe the design of an integrated steering stability controller considering the actuator saturation of yaw control in Section 3. In Section 4, a numerical simulation is carried out to verify the effectiveness of the designed controller, followed by our conclusions in Section 5.

2. Problem Formulation

During a turning manoeuvre by a vehicle, both yaw movement and roll movement are brought about; a 6-DOF turning dynamics model considering heave and roll movement of the sprung mass, left and right hop movement of the unsprung mass, and lateral and yaw movement of the whole vehicle is established in Figure 1, where z_s and θ are the vertical displacement and roll angle, respectively, of the sprung mass, z_{wl} and z_{wr} are the respective hop of the left and right unsprung mass, z_{rl} and z_{rr} are the respective vertical inputs of the left and right road, β and γ are the respective slip angle and yaw rate of the whole vehicle, m_s is the sprung mass, v is the vehicle velocity, F_y is the total lateral force of the four tires, h_g is the height of CG, k_s and c_s are the stiffness and damping coefficient of the unilateral (left or right, hereinafter) suspension springs and dampers, respectively, k_w and c_w are the respective stiffness and damping coefficient of the unilateral tire springs and

dampers, m_w is the unilateral mass of the unsprung mass, F_{yl} and F_{yr} are the respective lateral force of left and right tires, d is the half-tread, α_f and α_r are the respective slip angles of the front and rear wheels, δ_f is the steering angle of front wheel, a and b are the distance from the CG of the sprung mass to the front axle and rear axle, respectively, u_z and u_θ are respectively the equivalent vehicle body vertical force and roll moment, which are essentially determined by u_l and u_r, and u_l and u_r are the respective input forces of the left and right active suspensions. Conventionally, the control input forces u_l and u_r can be generated by linear electric motors.

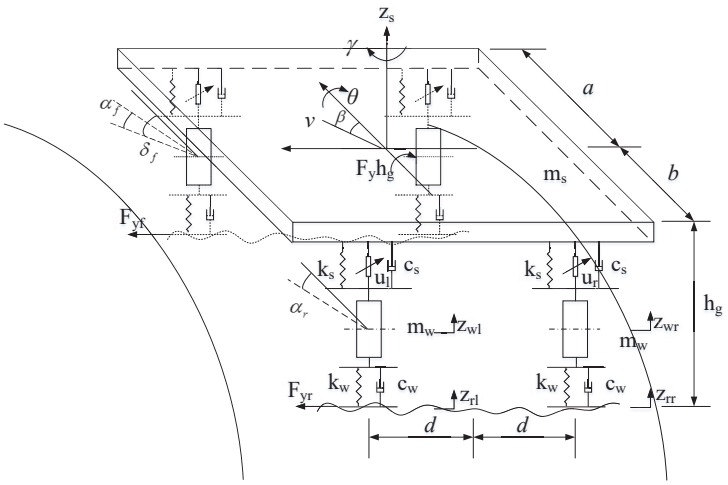

Figure 1. Vehicle model.

The corresponding dynamics can be formulated as follows:

$$m_s\ddot{z}_s + F_{sdl} + F_{sdr} + F_{ssl} + F_{ssr} = u_z \tag{1}$$

$$I_x\ddot{\theta} + d(F_{sdl} + F_{ssl}) - d(F_{sdr} + F_{ssr}) = u_\theta + F_y h_g \tag{2}$$

$$m_w\ddot{z}_{wl} - F_{sdl} - F_{ssl} + F_{wdl} + F_{wsl} = -u_l \tag{3}$$

$$m_w\ddot{z}_{wr} - F_{sdr} - F_{ssr} + F_{wdr} + F_{wsr} = -u_r \tag{4}$$

$$\dot{\beta} = -\frac{2(c_f + c_r)}{mv}\beta + \left(\frac{2(bc_r - ac_f)}{mv^2} - 1\right)\gamma + \frac{2c_f}{mv}\delta_f \tag{5}$$

$$\dot{\gamma} = \frac{2(bc_r - ac_f)}{I_z}\beta - \frac{2(a^2c_f + b^2c_r)}{I_z v}\gamma + \frac{2ac_f}{I_z}\delta_f + \frac{1}{I_z}M \tag{6}$$

where

$$\begin{cases} F_{wdl} = c_w(\dot{z}_{wl} - \dot{z}_{rl}) \\ F_{wdr} = c_w(\dot{z}_{wr} - \dot{z}_{rr}) \\ F_{wsl} = k_w(z_{wl} - z_{rl}) \\ F_{wsr} = k_w(z_{wr} - z_{rr}) \end{cases}, \quad \begin{cases} F_{sdl} = c_s\Delta\dot{y}_l \\ F_{sdr} = c_s\Delta\dot{y}_r \\ F_{ssl} = k_s\Delta y_l \\ F_{ssr} = k_s\Delta y_r \end{cases}, \quad \begin{cases} \Delta y_l = z_s + d\sin\theta - z_{wl} \\ \Delta y_r = z_s - d\sin\theta - z_{wr} \\ \Delta\dot{y}_l = \dot{z}_s + d\dot{\theta}\cos\theta - \dot{z}_{wl} \\ \Delta\dot{y}_r = \dot{z}_s - d\dot{\theta}\cos\theta - \dot{z}_{wr} \end{cases},$$

$$F_y = F_{yf}\cos\delta_f + F_{yr} = 2c_f\alpha_f\cos\delta_f + 2c_r\alpha_r,$$

$$K = \frac{m}{2L^2}\left(\frac{b}{c_f} - \frac{a}{c_r}\right), \quad L = a + b, \quad m = m_s + 2m_w,$$

$$\begin{cases} u_l + u_r = u_z \\ u_l d - u_r d = u_\theta \end{cases}, \quad \begin{cases} \alpha_f = \delta_f - \frac{a\gamma}{v} - \beta \\ \alpha_r = \frac{b\gamma}{v} - \beta \end{cases},$$

where F_{wdl} and F_{wdr} are the respective damper forces of the left tire and right tire, F_{wsl} and F_{wsr} are the respective spring forces of the left tire and right tire, F_{sdl} and F_{sdr} are the

respective damper forces of the left tire and right suspension, F_{ssl} and F_{ssr} are the respective spring forces of the left tire and right suspension, Δy_l and Δy_r are the dynamic deflection of the left and right suspension, respectively, c_f and c_r are the respective cornering stiffnesses of the single front and rear tires, L is the wheelbase, M is the yaw moment control input, which can be generated either by active wheel steering or braking force, and I_z and I_x are the respective inertial yaw and roll moments. For more detailed information about the physical meanings of these notations, readers can refer to [16,17,28] and the references therein.

The control problem can be depicted as follows: $\lim_{t\to\infty} z_s \to 0$ or bounded, $\lim_{t\to\infty} \theta \to 0$ or bounded, and $\lim_{t\to\infty} (\gamma - \gamma_r) \to 0$ or bounded, under the condition that z_{wl}, z_{wr} and β are bounded; γ_r is the reference yaw rate, which can be formulated as $\gamma_r = \frac{v/L}{1+Kv^2}\delta_f$.

3. Integrated Controller Design

Let $x_1 = z_s$, $x_2 = \dot{z}_s$, $x_3 = \theta$, $x_4 = \dot{\theta}$, $x_5 = z_{wl}$, $x_6 = \dot{z}_{wl}$, $x_7 = z_{wr}$, $x_8 = \dot{z}_{wr}$, $x_9 = \beta$, and $x_{10} = \gamma$; then, the vehicle dynamics can be reformulated as

$$\begin{aligned}
\dot{x}_1 &= x_2, \quad \dot{x}_2 = \frac{1}{m_s}(-F_{sdl} - F_{sdr} - F_{ssl} - F_{ssr} + u_z) \\
\dot{x}_3 &= x_4, \quad \dot{x}_4 = \frac{1}{I_x}(-d(F_{sdl} + F_{ssl}) + d(F_{sdr} + F_{ssr}) + F_y h_g + u_\theta) \\
\dot{x}_5 &= x_6, \quad \dot{x}_6 = \frac{1}{m_{wl}}(F_{sdl} + F_{ssl} - F_{wdl} - F_{wsl} - u_l) \\
\dot{x}_7 &= x_8, \quad \dot{x}_8 = \frac{1}{m_{wr}}(F_{sdr} + F_{ssr} - F_{wdr} - F_{wsr} - u_r) \\
\dot{x}_9 &= -\frac{2(c_f + c_r)}{mv}x_9 + \left(\frac{2(bc_r - ac_f)}{mv^2} - 1\right)x_{10} + \frac{2c_f}{mv}\delta_f \\
\dot{x}_{10} &= \frac{2(bc_r - ac_f)}{I_z}x_9 - \frac{2(a^2c_f + b^2c_r)}{I_z v}x_{10} + \frac{2ac_f}{I_z}\delta_f + \frac{1}{I_z}M
\end{aligned} \tag{7}$$

Accordingly, the integrated controller can be synthesised via the following three steps. Step 1: let $e_1 = x_1 - x_{1r}$, and $e_2 = x_2 - x_{2r}$, where x_{1r} is the reference value of x_1 and x_{2r} is the virtual control input; then,

$$\dot{e}_1 = \dot{x}_1 - \dot{x}_{1r} = e_2 + x_{2r} - \dot{x}_{1r}.$$

Choose $V_1 = \frac{1}{2}e_1^2$ as a Lyapunov candidate; its derivation along $\dot{e}_1$ yields

$$\dot{V}_1 = e_1(e_2 + x_{2r} - \dot{x}_{1r})$$

Take $x_{2r} = \dot{x}_{1r} - k_1 e_1$, where $k_1 > 0$ is the design parameter; then, we have

$$\dot{V}_1 = e_1 e_2 - k_1 e_1^2.$$

Choose $V_2 = V_1 + \frac{m_s}{2}e_2^2 + \frac{1}{2r_1}\tilde{m}_s^2$ as a Lyapunov candidate, where $\tilde{m}_s = \hat{m}_s - m_s$ and $\hat{m}_s$ is the estimation value of m_s; then, taking its deviation yields

$$\dot{V}_2 = e_1 e_2 - k_1 e_1^2 + e_2(-F_{sdl} - F_{sdr} - F_{ssl} - F_{ssr} + u_z - m_s\dot{x}_{2r}) + \frac{1}{r_1}\tilde{m}_s\dot{\hat{m}}_s.$$

Take

$$u_z = F_{sdl} + F_{sdr} + F_{ssl} + F_{ssr} + \hat{m}_s\dot{x}_{2r} - k_2 e_2 - e_1 \tag{8}$$

and the adaptation law

$$\dot{\hat{m}}_s = -r_1 e_2 \dot{x}_{2r}, \tag{9}$$

where $k_2 > 0$ and $r_1 > 0$ are design parameters; then, we have

$$\dot{V}_2 = -k_1 e_1^2 - k_2 e_2^2 \leq 0$$

which indicates that e_1, e_2 and $\tilde{m}_s$ are bounded. Taking the derivative of $\dot{V}_2$ leads to

$$\ddot{V}_2 = -2k_1 e_1(e_2 + x_{2r}) - 2k_2 e_2(\frac{1}{m_s}(-F_{sdl} - F_{sdr} - F_{ssl} - F_{ssr} + u_z) - \dot{x}_{2r}),$$

thus, $\dot{V}_2$ is uniformly continuous, conditional on x_{1r} and $\dot{x}_{1r} \in L_\infty$. Consequently, the error dynamics of e_1 and e_2 are asymptotically convergent to 0 with Lyapunov-like lemma.

Step 2: to facilitate the development of the control law, the following simplicities are used: $\theta_I = \frac{1}{I_x}$ and $f_\theta(x_\theta, \delta_f) = -d(F_{sdl} + F_{ssl}) + d(F_{sdr} + F_{ssr}) + F_y h_g$, where $x_\theta = (x_1, x_2, x_3, x_4, x_5, x_6, x_7, x_8)^T$. Let $e_3 = x_3 - x_{3r}$, $e_4 = x_4 - x_{4r}$, $\tilde{\theta}_I = \hat{\theta}_I - \theta_I$, where x_{3r} is the reference value of x_3, x_{4r} is the virtual control input, and $\hat{\theta}_I$ is the estimation of θ_I. Following a similar procedure as in Step 2, we can choose $V_4 = \frac{1}{2}e_3^2 + \frac{1}{2}e_4^2 + \frac{1}{2r_2}\tilde{\theta}_I^2$ as a Lyapunov function and take

$$x_{4r} = \dot{x}_{3r} - k_3 e_3 \tag{10}$$

$$u_\theta = -f_\theta(x_\theta, \delta_f) + \frac{1}{\hat{\theta}_I}(\dot{x}_{4r} - k_4 e_4 - e_3) \tag{11}$$

with the projection-type adaptation law [29–31]:

$$\begin{aligned} \dot{\hat{\theta}}_I &= Proj_{\hat{\theta}_I}(r_2 e_4(f_\theta(x_\theta, \delta_f) + u_\theta)) \\ &= \begin{cases} 0 & if\ \hat{\theta}_I = \theta_{I\max}\ and\ r_2 e_4(f_\theta(x_\theta, \delta_f) + u_\theta) > 0 \\ 0 & if\ \hat{\theta}_I = \theta_{I\min}\ and\ r_2 e_4(f_\theta(x_\theta, \delta_f) + u_\theta) < 0 \\ r_2 e_4(f_\theta(x_\theta, \delta_f) + u_\theta) & otherwise \end{cases} \end{aligned} \tag{12}$$

where $k_3 > 0$, $k_4 > 0$ and $r_2 > 0$ are design parameters, and $\theta_{I\max}$ and $\theta_{I\min}$ are the known maximum and minimum values of θ_I; then, we have

$$\dot{V}_4 = -k_3 e_3^2 - k_4 e_4^2 \leq 0.$$

Thus, e_3, e_4, and $\tilde{\theta}_I$ are bounded; taking the derivative of $\dot{V}_4$ further yields $\ddot{V}_4 = -2k_3 e_3(e_4 + x_{4r}) - 2k_4 e_4(\theta_I(f_\theta(x_\theta, \delta_f) + u_\theta) - \dot{x}_{4r})$, which is bounded on the condition that $\dot{x}_{3r}$ is bounded. Hence, $\dot{V}_4$ is uniformly continuous, and consequently e_3, $e_4 \to 0$, as $t \to \infty$ with Lyapunov-like lemma.

After u_z and u_θ are determined, the active suspension control input can be obtained as follows:

$$u_l = \frac{du_z + u_\theta}{2d}, \quad u_r = \frac{du_z - u_\theta}{2d}. \tag{13}$$

Step 3: for simplicity, let $f_\gamma(x_\gamma, \delta_f) = 2(bc_r - ac_f)x_9 - \frac{2(a^2c_f + b^2c_r)}{v}x_{10} + 2ac_f\delta_f$, where $x_\gamma = (x_9, x_{10})^T$; then, Equation (7) can be simplified as

$$\dot{x}_{10} = \frac{1}{I_z}(f_\gamma(x_\gamma, \delta_f) + M)$$

where the saturated control input can be presented as

$$M = sat(u_y) = \mathrm{sgn}(u_y) \cdot \min\{|u_y|, u_{\max}\}, \tag{14}$$

where u_y is the actuator demand input, $sat(u_y)$ is the actuator actual output, and $u_{max} > 0$ is the positive upper bound of the actuator.

We now take the state tracing error of x_{10} as $e_{10} = x_{10} - x_{10r}$, where x_{10r} is the reference value of x_{10}. Let $M_\Delta = M - u_y$, and pass it through a filter $\dot{\zeta} = -k_\zeta \zeta + M_\Delta$, where k_ζ is

the tuning parameter. The filter acts as an anti-windup compensator, thus, the actuator saturation M_Δ can be canceled out by feeding ζ back into the nominal control input, u_y [26].

Choosing a Lyapunov candidate $V_{10} = \frac{I_z}{2}e_{10}^2 + \frac{1}{2}\zeta^2$, we then have

$$\dot{V}_{10} = e_{10}(f_\gamma(x_\gamma, \delta_f) + M_\Delta + u_y - I_z\dot{x}_{10r}) - k_\zeta\zeta^2 + \zeta M_\Delta \tag{15}$$

We design the control law of u_y as

$$u_y = -f_\gamma(x_\gamma, \delta_f) + I_z\dot{x}_{10r} - k_{10}e_{10} - k_{11}\zeta, \quad k_{10} > 0. \tag{16}$$

Then, substituting (16) into (15) yields

$$\begin{aligned}
\dot{V}_{10} &= -k_{10}e_{10}^2 - k_\zeta\zeta^2 + e_{10}M_\Delta - k_{11}\zeta e_{10} + \zeta M_\Delta \\
&= -\frac{k_{10}}{3}e_{10}^2 + (e_{10}M_\Delta - \frac{k_{10}}{3}e_{10}^2) + (-\frac{k_{10}}{3}e_{10}^2 - \frac{k_\zeta}{3}\zeta^2 - k_{11}\zeta e_{10}) \\
&\quad -\frac{k_\zeta}{3}\zeta^2 + (\zeta M_\Delta - \frac{k_\zeta}{3}\zeta^2) \\
&= -\frac{k_{10}}{3}e_{10}^2 - (\sqrt{\frac{k_{10}}{3}}e_{10} - \sqrt{\frac{3}{4k_{10}}}M_\Delta)^2 + \frac{3}{4k_{10}}M_\Delta^2 \\
&\quad -\frac{1}{2}(\sqrt{k_{11}}e_{10} + \sqrt{k_{11}}\zeta)^2 - (-\frac{k_{11}}{2} + \frac{k_{10}}{3})e_{10}^2 - (-\frac{k_{11}}{2} + \frac{k_\zeta}{3})\zeta^2 \\
&\quad -\frac{k_\zeta}{3}\zeta^2 - (\sqrt{\frac{k_\zeta}{3}}\zeta - \sqrt{\frac{3}{4k_\zeta}}M_\Delta)^2 + \frac{3}{4k_\zeta}M_\Delta^2 \\
&\leq -(\frac{2k_{10}}{3} - \frac{k_{11}}{2})e_{10}^2 - (\frac{2k_\zeta}{3} - \frac{k_{11}}{2})\zeta^2 + (\frac{3}{4k_{10}} + \frac{3}{4k_\zeta})\bar{M}^2
\end{aligned}$$

where $\bar{M}$ is the upper bound of M_Δ. If we take $\rho = \min\{\frac{4k_{10}-3k_{11}}{3I_z}, \frac{4k_\zeta}{3} - k_{11}\}$, $\frac{2k_{10}}{3} > \frac{k_{11}}{2}$, and $\frac{2k_\zeta}{3} > \frac{k_{11}}{2}$, then

$$\dot{V}_{10} \leq -\rho V_{10} + \varepsilon \tag{17}$$

where $\varepsilon = (\frac{3}{4k_{10}} + \frac{3}{4k_\zeta})\bar{M}^2$. Integrating both sides of (17) generates

$$V_{10}(t) \leq \frac{\varepsilon}{\rho} + (V_{10}(0) - \frac{\varepsilon}{\rho})e^{-\rho t}$$

When $t \to \infty$, we have $V(\infty) \leq \frac{\varepsilon_0}{\rho}$, meaning that the signals e_{10} and ζ are ultimately bounded and the attraction domain of V_{10} can be adjusted to be smaller, with a smaller σ and a larger k_{10}.

The integrated controller design yields a fifth-order error dynamics system, while the original system is a tenth-order system. Hence, the zero dynamics contains five states. Setting $e_1 = e_3 = e_{10} = 0$ generates the following zero dynamics:

$$\dot{x}_0 = Ax_0 + Bz_0 + Cx_r + d_0 \tag{18}$$

where

$$x_0 = \begin{bmatrix} x_5 \\ x_6 \\ x_7 \\ x_8 \\ x_9 \end{bmatrix}, \quad A = \begin{bmatrix} 0 & 1 & 0 & 0 & 0 \\ -\frac{k_w}{m_w} & -\frac{c_w}{m_w} & 0 & 0 & 0 \\ 0 & 0 & 0 & 1 & 0 \\ 0 & 0 & -\frac{k_w}{m_w} & -\frac{c_w}{m_w} & 0 \\ 0 & 0 & 0 & 0 & -\frac{2(c_f+c_r)}{mv} \end{bmatrix},$$

$$B = \begin{bmatrix} 0 & 0 & 0 & 0 & 0 \\ \frac{k_w}{m_w} & \frac{c_w}{m_w} & 0 & 0 & 0 \\ 0 & 0 & 0 & 0 & 0 \\ 0 & 0 & \frac{k_w}{m_w} & \frac{c_w}{m_w} & 0 \\ 0 & 0 & 0 & 0 & \frac{2c_f}{mv} \end{bmatrix}, \quad z_0 = \begin{bmatrix} z_{rl} \\ \dot{z}_{rl} \\ z_{rr} \\ \dot{z}_{rr} \\ \delta_f \end{bmatrix},$$

$$C = \begin{bmatrix} 0 & 0 & 0 \\ -\frac{m_s}{2} & -\frac{I_x}{2d} & 0 \\ 0 & 0 & 0 \\ -\frac{m_s}{2} & \frac{I_x}{2d} & 0 \\ 0 & 0 & \frac{2(bc_r - ac_f)}{mv^2} - 1 \end{bmatrix}, \quad d_0 = \begin{bmatrix} 0 \\ \frac{F_y h_g}{2d} \\ 0 \\ -\frac{F_y h_g}{2d} \\ 0 \end{bmatrix}, \quad x_r = \begin{bmatrix} \dot{x}_{2r} \\ \dot{x}_{4r} \\ x_{10r} \end{bmatrix}.$$

It is easy to see that A is Hurwitz; accordingly the zero dynamics is stable.

The control scheme proposed in this paper is based on full-state feedback; thus, the full-state variable acquisition becomes a requirement. However, as certain states, especially for the vehicle sideslip angle β [32] and body roll angle θ, are not easy to measure directly by sensors, this requirement is somewhat demanding. In addition, the tire lateral force model is involved in the controller design; tire state measurement has been a difficult problem for many decades, and may lead to the limitation of the controller implementation in practice. For this problem, one possible solution is the use of 'smart tires' to measure the tire force directly, although this is expensive and complicated [33,34]; another feasible approach is to estimate the tire force by designing observers [35–37]. The flowchart of the proposed control scheme is provided in Figure 2.

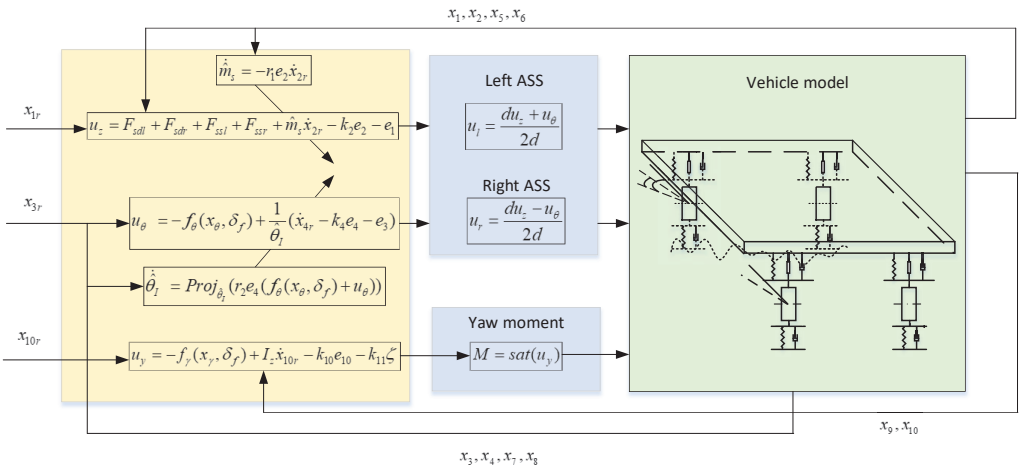

Figure 2. Control scheme flowchart.

4. Simulation Verification

To verify the effectiveness of the proposed integrated controller, numerical simulations are performed in this section. The parameters of the vehicle model used for the simulations are provided in Table 1, while the parameters of the proposed controller are provided in Table 2. Two different simulation scenarios are performed, with the following state initializations: $x_1(0) = 0.1$ m, $x_3(0) = 0.1$ rad, $\hat{\theta}_I(0) = \frac{1}{500}$ kg^{-1}·m^{-2}, and the rest set to 0, with a constant vehicle speed of 50 m/s. Using a sampling time of 0.001 s and the aforementioned scenario settings, a detailed elaboration is presented with in following Sections 4.1 and 4.2. To comparatively show the effects of the proposed controller, another controller from [17]

$$\Psi = \begin{cases} M = I_z \dot{\gamma}_r - k_\gamma I_z (\gamma - \gamma_r), & k_\gamma > 0 \\ u_\theta = -k_\theta I_x \dot{\theta}, & k_\theta > 0 \\ u_z = -k_z m_s \dot{z}_s, & k_z > 0 \end{cases}$$

is used as a contrast, with the tuning parameters k_γ, k_θ, and k_z assigned as shown in Table 2. In these comparative simulations, all environmental parameters are set to be the same except for the different controller parameters.

Table 1. Parameters of the vehicle model.

Parameter	Value	Parameter	Value
m_s	1110 kg	m_w	2×30 kg
I_x	440.6 kg·m^2	I_z	1343.1 kg·m^2
c_s	2×4000 Ns/m	k_s	$2 \times 28{,}000$ N/m
c_w	2×1000 Ns/m	k_w	$2 \times 232{,}000$ N/m
c_f	22,010 N/rad	c_r	22,010 N/rad
h_g	0.54 m	d	0.74 m
a	1.04 m	b	1.56 m
θ_{Imax}	1/400 kg^{-1}·m^{-2}	θ_{Imin}	1/600 kg^{-1}·m^{-2}

Table 2. Parameters of the proposed controller and the compared controller.

Parameter	Value	Parameter	Value	Parameter	Value
k_1	1	k_2	10,000	k_3	10
k_4	1	k_{10}	100	k_ζ	10
r_0	10	σ	0.01	r_1	5000
r_2	0.001	k_{11}	0.1	k_γ, k_θ, k_z	10

4.1. Scenario 1: Square-Wave Front Wheel Input with Flat Road Surface

In this scenario, the vehicle runs on a flat road under a square-wave front road wheel input with 0.5 Hz frequency and 0.01 rad amplitude. The simulation results are exhibited in Figures 3–10.

The vehicle body vertical displacement and acceleration are illustrated in Figures 3 and 4, respectively, from which it can be seen that the proposed controller can render the heave motion of the sprung mass as zero, asymptotically stable, and decrease the vertical acceleration dramatically, hence, improving vehicle ride comfort. Although the vertical displacement under the proposed controller converges slower than under the comparative controller Ψ, the vertical acceleration converges much faster, effectively improving ride comfort, as the vertical acceleration, rather than the displacement, is the main comfort index.

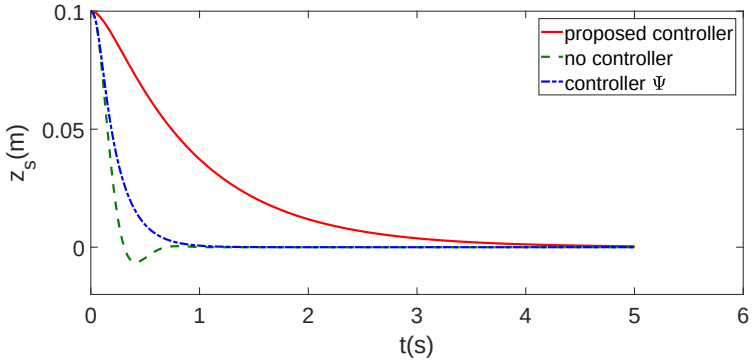

Figure 3. Vehicle body vertical displacement.

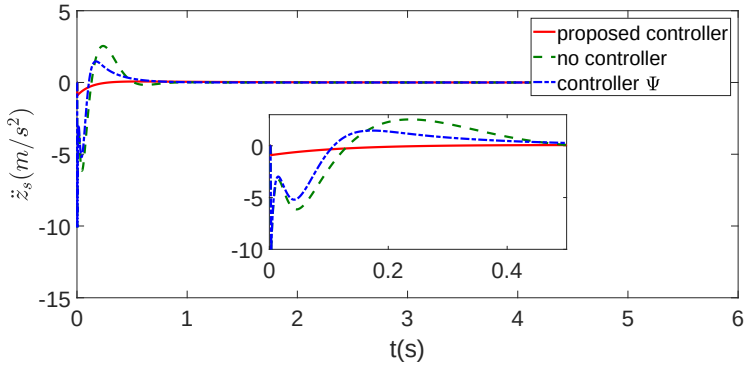

Figure 4. Vehicle body vertical acceleration.

Figures 5 and 6 exhibit the vehicle roll angle and roll angular acceleration. From Figures 5 and 6, it can be seen that the roll motion can be stabilized using the proposed integrated controller, while controller Ψ can hardly realize it. The roll and heave control input, that is, the active suspension input force, is presented in Figure 7.

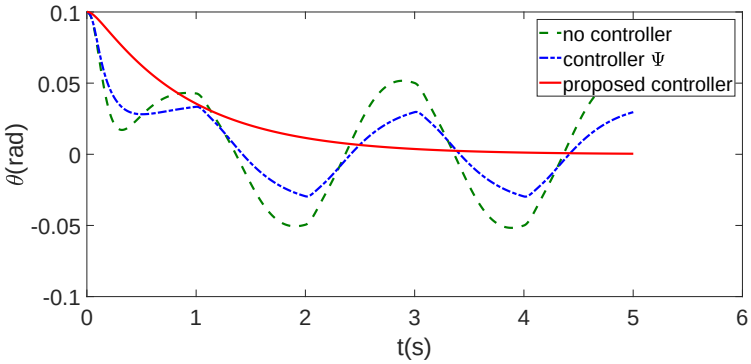

Figure 5. Vehicle roll angle.

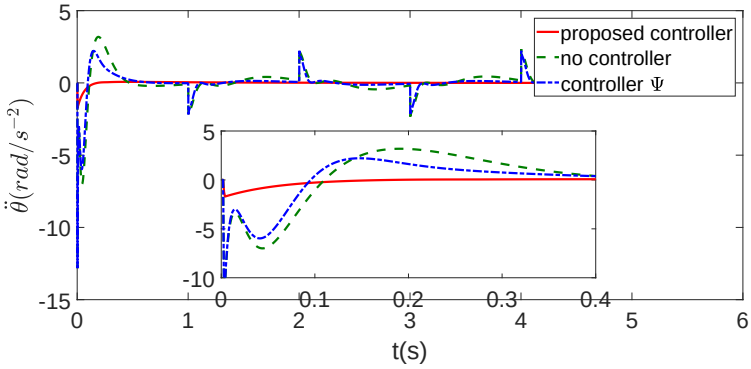

Figure 6. Vehicle roll angular acceleration.

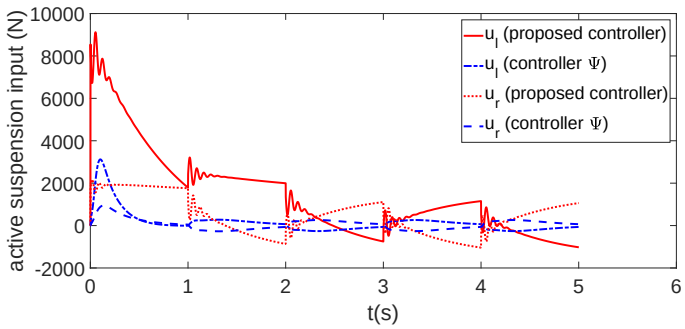

Figure 7. Active suspension input.

The vehicle sideslip angle and yaw rate are illustrated in Figures 8 and 9, supposing that the maximum yaw control effort satisfies $u_{max} = 1000$ N. Figure 9 indicates that lower performance degradation can be guaranteed with the proposed controller when saturation of the yaw control actuator occurs. In addition, Figure 8 shows that the vehicle under the proposed controller possesses a lower sideslip angle compared with respect to the compared controller, making for more stable lateral motion with the proposed controller.

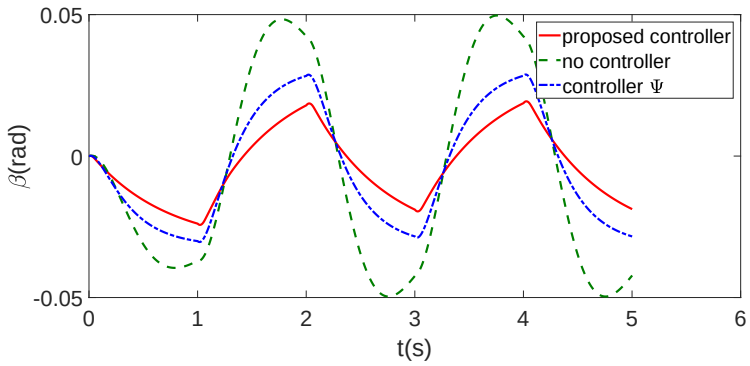

Figure 8. Vehicle sideslip angle.

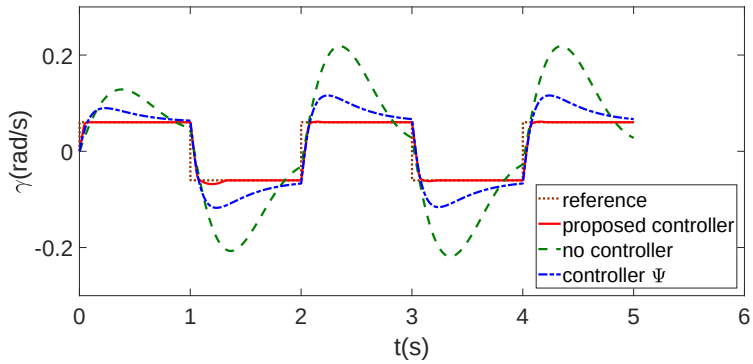

Figure 9. Vehicle yaw rate.

The yaw motion control input is illustrated in Figure 10, and the corresponding state of the anti-windup compensator ζ is illustrated in Figure 11. From these two figures, it can be seen that when the control input reaches the actuator limitation u_{max}, the state of the anti-windup compensator ζ accordingly increases its value such that the control input decreases by feeding ζ back into the control input u_y, consequently reducing the impact of actuator saturation on control performance.

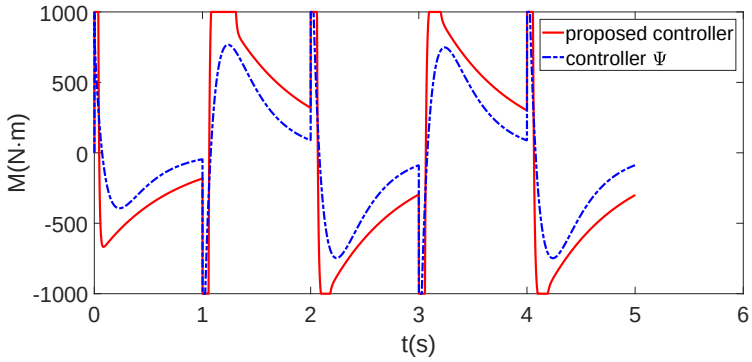

Figure 10. Yaw motion control input.

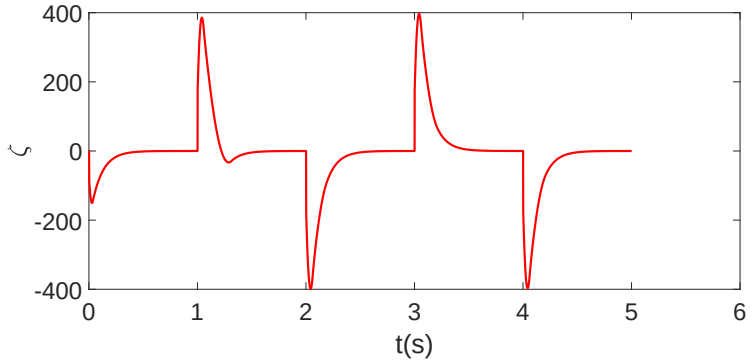

Figure 11. State of the anti-windup compensator.

4.2. Scenario 2: J-Turn Front Wheel Input with Sinusoidal Vertical Road Surface

To further demonstrate the effectiveness of the proposed controller on steering stability under more severe circumstances, another scenario involving J-turn front wheel input and a sinusoidal vertical road surface was used as an additional simulation environment. The J-turn manoeuvre represents a type of sharp turning operation; the corresponding front wheel steering angle input is provided in Figure 12. The sinusoidal vertical road input is set as $z_{rl} = 0.01sin(\pi t)$ for the left wheel and $z_{rr} = 0.01cos(\pi t)$ for the right wheel. The controller parameters are kept identical to those in Section 4.1.

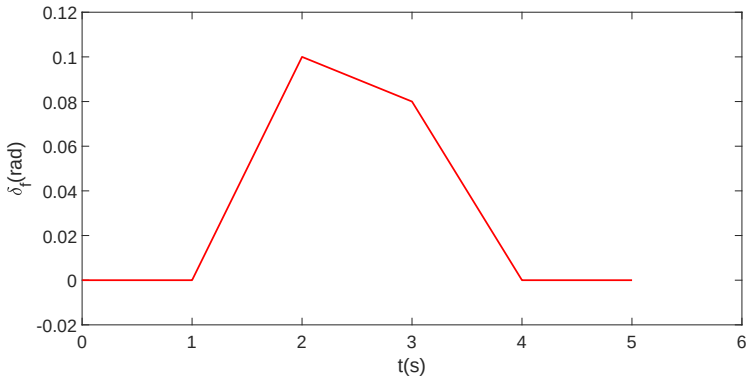

Figure 12. Front wheel input for J-turn simulation.

The simulation results are shown in Figures 13–21. Figures 13–17 show the sprung mass dynamics and the corresponding active suspension control inputs, while Figures 18 and 19 show the the later motion dynamics. A detailed elaboration is not provided here due to the similarity between this scenario and the first scenario described in Section 4.1.

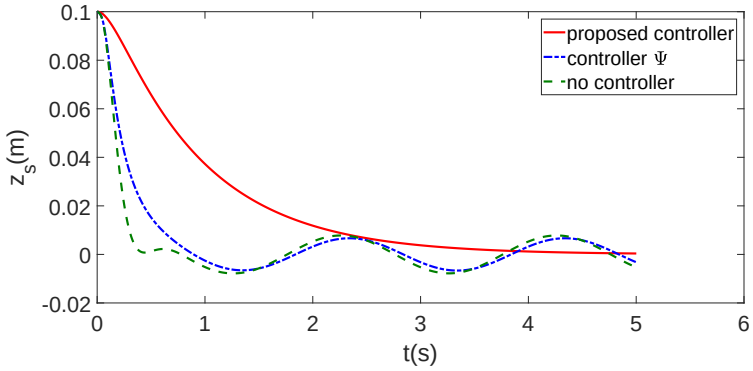

Figure 13. Vehicle body vertical displacement.

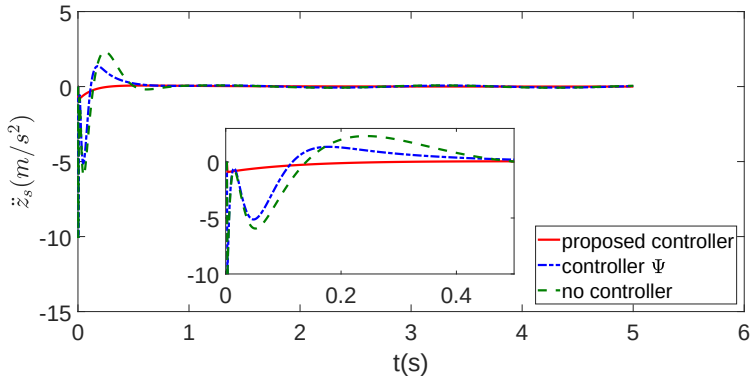

Figure 14. Vehicle body vertical acceleration.

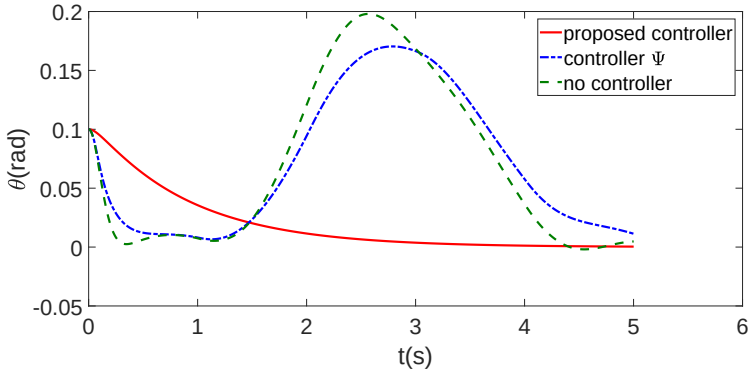

Figure 15. Vehicle roll angle.

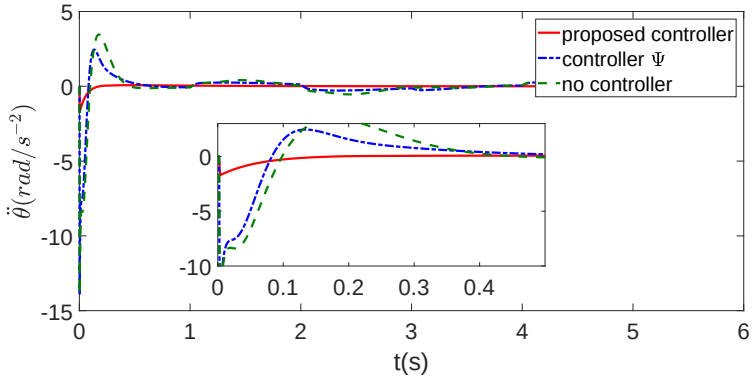

Figure 16. Vehicle roll angular acceleration.

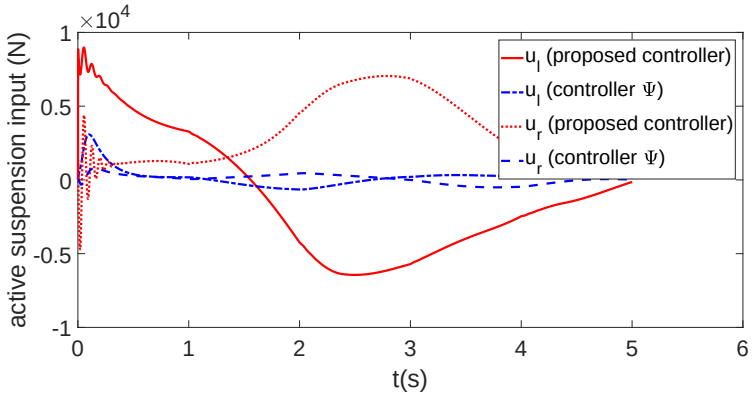

Figure 17. Active suspension input.

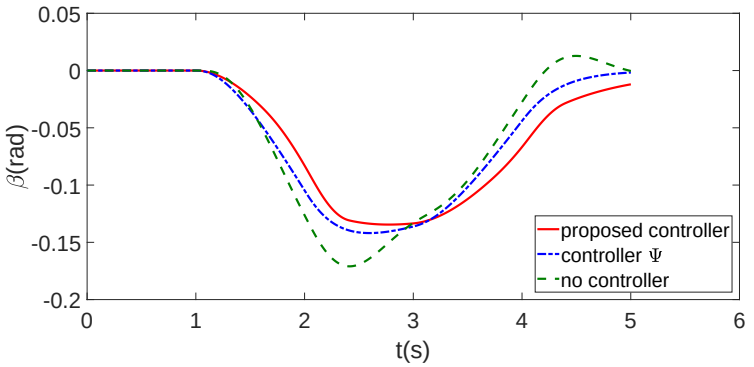

Figure 18. Vehicle sideslip angle.

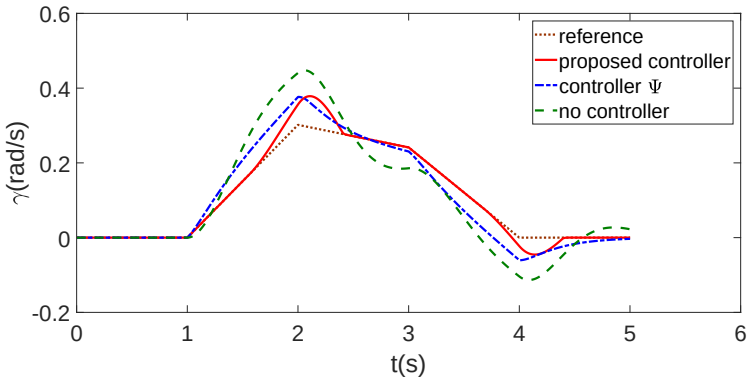

Figure 19. Vehicle yaw rate.

The yaw motion control input M together with the state of the anti-windup compensator ζ are shown in Figures 20 and 21. Similarly, it can be seen that by feeding back ζ the controller saturation can be alleviated, thereby reducing the control impact from actuator saturation.

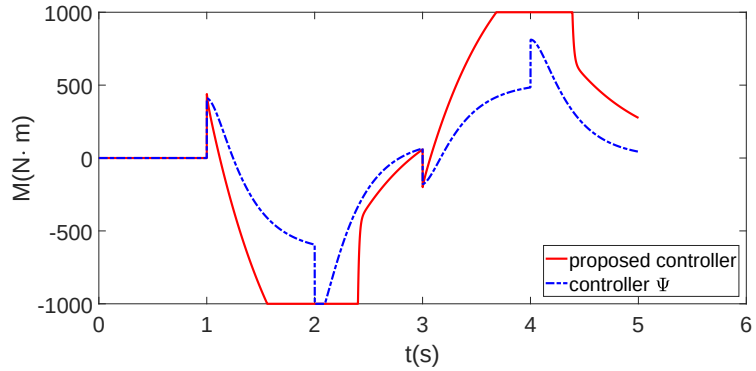

Figure 20. Yaw moment control input.

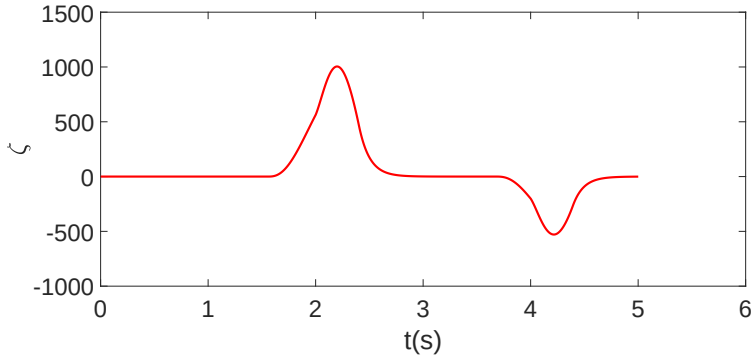

Figure 21. State of the anti-windup compensator.

In short, the proposed controller can provide lower vehicle body vertical and roll angle acceleration, thus improving vehicle ride comfort, and simultaneously guaranteeing alleviation of yaw rate tracking performance degradation caused by actuator saturation.

It should be noted that the yaw rate is taken as the controlled state and the sideslip angle is not considered in the proposed controller. On the one hand, the zero dynamics of the sideslip angle is proven to be stable by Equation (18); on the other hand, from [38], we know that a small lateral velocity and sideslip angle can be maintained under the condition that yaw rate is controlled to track its reference value. Furthermore, the road condition is not considered in this paper; for pracitical implementation, the refence yaw rate can be replaced by

$$\gamma_r = \begin{cases} \frac{v/L}{1+Kv^2}\delta_f & if \left|\frac{v/L}{1+Kv^2}\delta_f\right| < \mu g \\ \frac{\mu g}{v}\mathrm{sgn}(\frac{v/L}{1+Kv^2}\delta_f) & otherwise \end{cases}. \tag{19}$$

5. Conclusions

In this paper, an integrated vehicle dynamics under steering manoeuvre is established, initially considering the steering influence on the vehicle body roll motion; a corresponding integrated controller is then proposed. Our simulation results indicate that the proposed integrated controller can stabilize vehicle roll motion caused by steering and simultaneously alleviate vehicle yaw rate tracking performance degradation caused by yaw control actuator saturation. The implementation of the proposed controller will be the focus of our future research.

Author Contributions: Conceptualization, J.Z.; Data curation, J.Z.; Formal analysis, J.Z.; Funding acquisition, J.Z.; Investigation, M.W.; Methodology, M.W.; Project administration, M.W.; Resources, M.W. All authors have read and agreed to the published version of the manuscript.

Funding: This research was funded by the Guangzhou Science and Technology Plan Project (202201020173, 202201010475).

Institutional Review Board Statement: Not applicable.

Informed Consent Statement: Not applicable.

Data Availability Statement: Not applicable.

Conflicts of Interest: The authors declare no conflict of interest.

References

1. Hu, J.; Wang, Y.; Fujimoto, H.; Hori, Y. Robust yaw stability control for in-wheel motor electric vehicles. *IEEE/ASME Trans. Mechatron.* **2017**, *22*, 1360–1370. [CrossRef]
2. Sun, W.; Tang, S.; Gao, H.; Zhao, J. Two time-scale tracking control of nonholonomic wheeled mobile robots. *IEEE Trans. Control Syst. Technol.* **2016**, *24*, 2059–2069. [CrossRef]
3. Choi, M.; Choi, S.B. Model predictive control for vehicle yaw stability with practical concerns. *IEEE Trans. Veh. Technol.* **2014**, *63*, 3539–3548. [CrossRef]
4. Zhang, J.; Sun, W.; Du, H. Integrated motion control scheme for four-wheel-independent vehicles considering critical conditions. *IEEE Trans. Veh. Technol.* **2019**, *68*, 7488–7497. [CrossRef]
5. Li, B.; Du, H.; Li, W.; Zhang, Y. Side-slip angle estimation based lateral dynamics control for omni-directional vehicles with optimal steering angle and traction/brake torque distribution. *Mechatronics* **2015**, *30*, 348–362. [CrossRef]
6. Zhao, H.; Gao, B.; Ren, B.; Chen, H. Integrated control of in-wheelmotor electric vehicles using a triple-step nonlinear method. *J. Frankl. Inst.* **2015**, *352*, 519–540. [CrossRef]
7. Pugi, L.; Favilli, T.; Berzi, L.; Cappa, M.; Pierini, M. An Optimal Torque and Steering Allocation Strategy for Stability Control of Road Vehicles. In Proceedings of the 21st IEEE International Conference on Environment and Electrical Engineering and 2021 5th IEEE Industrial and Commercial Power System Europe, EEEIC/I and CPS Europe 2021—Proceedings, Bari, Italy, 7–10 September 2021.
8. Allotta, B.; Pugi, L.; Bartolini, F.; Cangioli, F.; Colla, V. Comparison of different control approaches aiming at enhancing the comfort of a railway vehicle. In Proceedings of the IEEE/ASME International Conference on Advanced Intelligent Mechatronics, Montreal, QC, Canada, 6–9 July 2010; pp. 676–681.
9. Cairano, S.D.; Tseng, H.E.; Bernardini, D.; Bemporad, A. Vehicle yaw stability control by coordinated active front steering and differential braking in the tire sideslip angles domain. *IEEE Trans. Control Syst. Technol.* **2017**, *21*, 1236–1248. [CrossRef]
10. Sun, W.; Pan, H.; Gao, H. Filter-based adaptive vibration control for active vehicle suspensions with electro-hydraulic actuators. *IEEE Trans. Veh. Technol.* **2016**, *65*, 4619–4626. [CrossRef]
11. Zhang, J.; Sun, W.; Liu, Z.; Zeng, M. Comfort braking control for brake-by-wire vehicles. *Mech. Syst. Signal Process.* **2019**, *133*, 106255. [CrossRef]
12. Zhang, J.; Sun, W.; Jing, H. Nonlinear Robust Control of Antilock Braking Systems Assisted by Active Suspensions for Automobile. *IEEE Trans. Control Syst. Technol.* **2019**, *27*, 1352–1359. [CrossRef]
13. Sun, W.; Pan, H.; Zhang, Y.; Gao, H. Multi-objective control for uncertain nonlinear active suspension systems. *Mechtronics* **2014**, *24*, 318–327. [CrossRef]
14. Sun, W.; Gao, H.; Yao, B. Adaptive robust vibration control of full-car active suspensions with electrohydraulic actuators. *IEEE Trans. Control Syst. Technol.* **2013**, *21*, 2417–2422. [CrossRef]
15. Riofrio, A.; Sanz, S.; Boada, M.J.L.; Boada, B.L. A lqr-based controller with estimation of road bank for improving vehicle lateral and rollover stability via active suspension. *Sensors* **2017**, *17*, 2318. [CrossRef]
16. Her, H.; Suh, J.; Yi, K. Integrated control of the differential braking, the suspension damping force and the active roll moment for improvement in the agility and the stability. *Proc. Inst. Mech. Eng. Part D J. Automob. Eng.* **2015**, *229*, 1145–1157. [CrossRef]
17. Chou, H.; D'andréa-Novel, B. Global vehicle control using differential braking torques and active suspension forces. *Veh. Syst. Dyn.* **2005**, *43*, 261–284. [CrossRef]
18. Cao, J.; Jing, L.; Guo, K.; Yu, F. Study on integrated control of vehicle yaw and rollover stability using nonlinear prediction model. *Math. Probl. Eng.* **2013**, *2013*, 643548. [CrossRef]
19. Hsin, G.; Kyongil, K.; Wang, B. Comprehensive path and attitude control of articulated vehicles for varying vehicle conditions. *Int. J. Heavy Veh. Syst.* **2017**, *24*, 65–95.
20. Saeedi, M.A. A new robust combined control system for improving manoeuvrability, lateral stability and rollover prevention of a vehicle. *Proc. Inst. Mech. Eng. Part K J. Multi-Body Dyn.* **2020**, *1*, 198–213. [CrossRef]
21. Williams, D.E.; Haddad, W.M. Nonlinear control of roll moment distribution to influence vehicle yaw characteristics. *IEEE Trans. Control Syst. Technol.* **1995**, *3*, 110–116. [CrossRef]
22. Sun, W.; Zhao, Z.; Gao, H. Saturated adaptive robust control for active suspension systems. *IEEE Trans. Ind. Electron.* **2013**, *60*, 3889–3896. [CrossRef]
23. Hong, Y.; Yao, B. A globally stable high-performance adaptive robust control algorithm with input saturation for precision motion control of linear motor drive systems. *IEEE/ASME Trans. Mechatron.* **2007**, *12*, 198–207. [CrossRef]
24. Tarbouriech, S.; Turner, M. Anti-windup design: An overview of some recent advances and open problems. *IET Control Theory Appl.* **2009**, *3*, 1–19. [CrossRef]

25. Wen, C.; Zhou, J.; Liu, Z.; Su, H. Robust adaptive control of uncertain nonlinear systems in the presence of input saturation and external disturbance. *IEEE Trans. Autom. Control* **2011**, *56*, 1672–1678. [CrossRef]
26. Sun, L.; Zheng, Z. Disturbance-observer-based robust backstepping attitude stabilization of spacecraft under input saturation and measurement uncertainty. *IEEE Trans. Ind. Electron.* **2017**, *64*, 7994–8002. [CrossRef]
27. Wang, F.; Zou, Q.; Zong, Q. Robust adaptive backstepping control for an uncertain nonlinear system with input constraint based on lyapunov redesign. *Int. J. Control Autom. Syst.* **2017**, *15*, 212–225. [CrossRef]
28. Zhang, J.; Sun, W.; Feng, Z. Vehicle yaw stability control via $\mathcal{H}_\infty$ gain scheduling. *Mech. Syst. Signal Process.* **2018**, *106*, 62–75. [CrossRef]
29. Yao, J.; Deng, W.; Jiao, Z. Adaptive control of hydraulic actuators with LuGre model based friction compensation. *IEEE Trans. Ind. Electron.* **2015**, *62*, 6469–6477. [CrossRef]
30. Sun, W.; Zhang, Y.; Huang, Y.; Gao, H.; Kaynak, O. Transient-performance-guaranteed robust adaptive control and its application to precision motion control systems. *IEEE Trans. Ind. Electron.* **2016**, *63*, 6510–6518. [CrossRef]
31. Chen, Z.; Yao, B.; Wang, Q. μ-synthesis based adaptive robust control of linear motor driven stages with high-frequency dynamics: A case study with comparative experiments. *IEEE/ASME Trans. Mechatron.* **2015**, *20*, 1482–1490. [CrossRef]
32. Zhang, H.; Huang, X.; Wang, J.; Karimi, H.R. Robust energy-to-peak sideslip angle estimation with applications to ground vehicles. *Mechatronics* **2015**, *30*, 338–347. [CrossRef]
33. Yi, J. A piezo-sensor-based "smart tire" system for mobile robots and vehicles. *IEEE/ASME Trans. Mechatron.* **2008**, *13*, 95–103. [CrossRef]
34. Cheli, F.; Leo, E.; Melzi, S.; Sabbioni, E. On the impact of 'smart tyres' on existing ABS/EBD control systems. *Veh. Syst. Dyn.* **2010**, *48*, 255–270. [CrossRef]
35. Wang, R.; Wang, J. Actuator-redundancy-based fault diagnosis for four-wheel independently actuated electric vehicles. *IEEE Trans. Intell. Transp. Syst.* **2014**, *15*, 239–249. [CrossRef]
36. Wei, X.; Wu, Z.; Karimi, H.R. Disturbance observer-based disturbance attenuation control for a class of stochastic systems. *Automatica* **2016**, *63*, 21–25. [CrossRef]
37. Wang, R.; Wang, J. Fault-tolerant control for electric ground vehicles with independently-actuated in-wheel motors. *J. Dyn. Syst. Meas. Control* **2012**, *134*, 021014. [CrossRef]
38. Zhou, H.; Liu, Z. Vehicle yaw stability-control system design based on sliding mode and backstepping control approach. *IEEE Trans. Veh. Technol.* **2010**, *59*, 3674–3678. [CrossRef]